

https://dspace.org/

Effect of nanoscale surface oxide layers on the cold spray of commercially pure titanium and Ti6Al4V powders

M Vandadi; T Bond; T.K Asumadu; Desmond Klenam; N Rahbar ...

ELSEVIER SCIENCE BV
https://hdl.handle.net/10539/46831
WOS

Downloaded from a DSpace repository. https://dspace.org/

Computational Materials Science 246 (2025) 113454

Contents lists available at ScienceDirect

Computational Materials Science

journal homepage: www.elsevier.com/locate/commatsci

Full length article

Effect of nanoscale surface oxide layers on the cold spray of commercially pure titanium and Ti–6Al–4V powders

Mobin Vandadi [a], Trevor Bond [b], Tabiri K. Asumadu [c,d,e], Desmond Klenam [f], Nima Rahbar [a,b,*], Winston Soboyejo [c]

[a] Department of Civil and Environmental Engineering, Worcester Polytechnic Institute, Worcester, MA, USA
[b] Materials Program, Department of Mechanical Engineering, Worcester Polytechnic Institute, Worcester, MA 01609, USA
[c] State of University of New York Polytechnic Institute, College of Engineering, 100 17 Seymour Road, Utica, NY 13502, USA
[d] Department of Materials Engineering, Kwame Nkrumah University of Science and Technology, Kumasi, Ghana
[e] Department of Materials Engineering, Sunyani Technical University, Box 206, Sunyani, Ghana
[f] School of Chemical and Metallurgical Engineering & Academic Development Unit, University of the Witwatersrand, 1 Jan Smuts Avenue, WITS 2001, Johannesburg, South Africa

ARTICLE INFO

Keywords:
Cold spray
Titanium alloys
Oxide layer
Molecular dynamics
Finite element simulations
Deformation mechanisms

ABSTRACT

This study presents a numerical analysis of commercially pure Ti and Ti–6Al–4V powders under cold spray conditions. The primary objectives are to investigate the deformation mechanisms, splat formation during the cold spray process, and the impact of the oxide layer. Initially, structural data obtained from transmission electron microscopy (TEM) are used to model the oxide structure through molecular dynamics simulations. Subsequently, molecular dynamics are employed to evaluate the mechanical properties of the oxide layer. Finally, finite element-based models are utilized to analyze and visualize the deformation process and the thermal effects when single Ti/Ti–6Al–4V particles impact substrates of the same material. These results offer an understanding of splat evolution and oxide residuals that affect particle attachment to substrates of the same material. The implications of these findings for designing and developing robust cold-sprayed Ti alloys are briefly discussed, emphasizing the potential for optimizing cold-spray process parameters and enhancing coating quality.

1. Introduction

Titanium and its alloys have garnered significant attention due to their unique combination of functional and structural properties, including an excellent strength-to-weight ratio, high resistance to oxidation and corrosion, biocompatibility, and low toxicity [1–10]. These attributes make titanium highly desirable for applications in aerospace, biomedical, and corrosive environments. However, pure titanium has limitations, such as low fatigue and yield strengths and intermediate fracture toughness values [7]. To address these limitations, titanium alloys such as Ti–6Al–4V have been developed by alloying titanium with elements that stabilize the α and β phases, resulting in improved mechanical properties suitable for aerospace and biomedical applications [8–10].

In recent years, there has been growing interest in developing repair methods for aging structures, with additive manufacturing techniques gaining increasing attention [11]. One such additive manufacturing method is the cold spray (CS) technique. Cold spray is a promising method for depositing metallic coatings and repairing damaged components, offering advantages such as low-temperature processing and the ability to retain desirable material properties.

Cold spray technology, developed in the mid-1980s in Novosibirsk, Russia, has since attracted significant research interest [1,12–21]. Numerous parameters affect the structural integrity of the cold spray process, including powder or particle size, feeding rate, gas type (nitrogen or helium) and temperature, gas pressure, and the distance between the nozzle outlet and the substrate. Optimizing these parameters enhances deposition efficiency. Furthermore, controlling particle velocity is crucial, as it must be high enough to ensure bonding between the substrate and the particles. Low velocities lead to elastic rebounding of particles, while high velocities cause erosion and material loss in both the substrate and the powder [1,14].

During the impact of metallic powders, the topical oxide layer is initially cracked and removed from the interface due to the jetting phenomenon. Subsequently, the substrate and particles form geometrical interlocking and metallic bonding due to plastic deformations [22,23]. Localized melting during and after impact results in temperature increases sufficient for recrystallization, forming new dislocation-free grains with improved ductility [24]. Understanding these phenomena and their dependence on cold spray parameters is crucial for optimizing

* Correspondence to: 100 Institute Rd., Worcester, MA 01609, USA.
E-mail addresses: nrahbar@wpi.edu (N. Rahbar), soboyew@sunypoly.edu (W. Soboyejo).

https://doi.org/10.1016/j.commatsci.2024.113454
Received 25 July 2024; Received in revised form 8 October 2024; Accepted 13 October 2024
Available online 28 October 2024
0927-0256/© 2024 Published by Elsevier B.V.

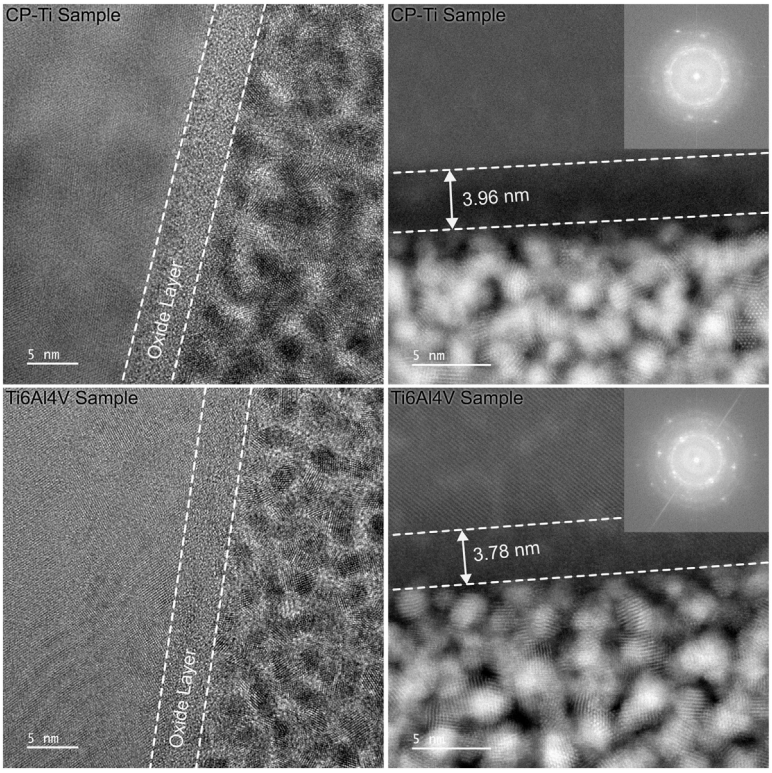

Fig. 1. High-Resolution Transmission Electron Microscopy image of the topical oxide formed on grade 2 and 5 titanium. The thickness of the oxide layer in both cases is approximately 4 nm and the fast-Fourier transform shows that it has an amorphous structure.

the process and achieving desirable coating properties. Insights into deformation mechanisms, cracking phenomena, and splat formation can contribute to developing robust Ti-based materials and advancing cold spray technology for various industrial applications.

This study investigates the influence of topical oxide layers on the deformation, heating, and splat formation that facilitate the bonding of commercially pure Ti and Ti–6Al–4V powders during the cold spray process onto substrates of the same material. Molecular dynamics simulations are used to calculate the stress–strain behavior of the oxide layer. These properties are then incorporated into finite element analyses of single-particle cold spray events to quantify the influence of the oxide layer on the cold spray process.

2. Methods

2.1. Material characterization

High-Resolution Transmission Electron Microscopy (HRTEM) was employed to characterize the oxide layer on both Commercially Pure Ti (CP-Ti) and Ti–6Al–4V powders. This analysis serves to quantify the oxide layer's thickness and identify its crystal structure. After exposure to ambient air for a few hours, the oxidation rate at room temperature stabilizes, as indicated by the logarithmic law of oxidation kinetics and experimental studies [25,26], making the measured oxide thickness a reliable estimate of its stable value.

Fig. 1 presents HRTEM images of the oxide layer on both types of titanium powders. Fast-Fourier Transform (FFT) analysis reveals that the oxide layer is amorphous in structure, with a thickness of approximately 4 nm for both powder types. Despite the presence of other elements in Ti–6Al–4V powders, Scanning Transmission Electron Microscopy (STEM) images did not detect significant quantities of these elements in the oxide layer, suggesting that the oxide structure is consistent across both types of titanium powders.

2.2. Molecular dynamics simulation

As described in the previous section, the titanium surface oxide exhibits an amorphous structure. Thus, a representative amorphous oxide structure is needed to calculate the mechanical properties of this layer. A $10 \times 10 \times 10$ nm^3 rutile oxide structure was initially chosen. According to Zhang et al. [27], the density of amorphous titanium oxide is 3.74 g/cm^3, which is lower than the density of rutile oxide (4.25 g/cm^3).

All molecular dynamics (MD) simulations were conducted using the LAMMPS code [28]. The force field employed was the second moment tight binding QEq (SMTB-Q) [29], which includes interactions among three components: electrostatic interactions (E_{ES}), oxygen–oxygen interactions (E_{OO}), and short-range metal–oxygen interactions (E_{MO}). The charge equilibration (QEq) method, combined with the force field, adjusted the partial charges of each atom based on interactions with neighboring atoms [30].

Initially, the box size was set to 1.5 times the necessary size for amorphous titanium oxide density, and the system temperature was set to 5000 K. This high temperature ensures that all atoms are free to move within the system. Subsequently, the 'fix deform' command was used to adjust the density of the system to match that of amorphous titanium oxide over 3 ns with a timestep of 1 fs. The system was then maintained at 5000 K and a constant volume for equilibration using the NPT ensemble over 2 ns. Following this, the system was linearly cooled to room temperature, and finally, it was thermally equilibrated at 300 K for 1 ns. Periodic boundary conditions were applied in all directions throughout these steps.

Due to the inherent randomness of the ensembles, each repetition of this procedure produces a different structure. Key factors influencing the final structure include the cooling rate and the annealing time at 1.5 times the box size. Therefore, three cooling rates (1 K/ps, 2 K/ps, and 4 K/ps) and three initial annealing times (1 ns, 2 ns, and 4 ns) were investigated. The Berendsen thermostat's exponential

decay during cooling was set to 1 to ensure adherence to the preset temperature profile.

The nine obtained amorphous samples were analyzed using the radial distribution function (RDF) and compared with the experimentally obtained RDFs (Ti–Ti) from Zhang et al. [27]. The structure with the closest main peak position and the full width at half maximum was selected for further analysis.

The chosen amorphous titanium oxide structure was then used in subsequent molecular dynamics simulations to estimate the stress–strain behavior of the film. A block with dimensions of 3.8 nm in height and 3 nm in length and width was created by replicating and removing extra atoms. Periodic boundary conditions were applied in the 'x' and 'y' directions to create a repeating system, while the 'z' direction was shrink-wrapped to prevent atoms from exiting the boundary. The structure was energetically minimized using the conjugate gradient method and brought to thermal equilibrium using both canonical (NVT) and isothermal–isobaric (NPT) ensembles over 1 ns.

After equilibration and stabilization, the structure was subjected to uniaxial tension in the 'z' direction at strain rates of 10^4 s^{-1} and 10^5 s^{-1}. According to Rida et al. [31], strain rates above 10^5 s^{-1} significantly influence Young's modulus and results from molecular dynamics simulations. The stress–strain curve of the amorphous titanium oxide film was then computed based on the applied deformation.

2.3. Finite element modeling

To simulate the cold spray process at the particle–substrate interface, a numerical model was developed using the ABAQUS/Explicit finite element software package (Dassault Systèmes, Vélizy-Villacoublay, France) with a Lagrangian formulation. The Arbitrary Lagrangian Eulerian (ALE) formulation was employed for both the particle and substrate to capture large deformations accurately.

The substrate was modeled as a cylinder, and the particle was represented as a perfect sphere impacting the substrate along the normal direction. Due to the axisymmetric nature of the problem, only a quarter of the system was simulated. The dimensions of the substrate, including its height and radius, were based on the average particle radius to ensure that stress distributions were accurately represented.

To incorporate the topical oxide layer, shells with a thickness of 3.8 nm – consistent with the observed nanoscale titanium dioxide layer – were added around the particles and the top layer of the substrate.

Interactions between the particle and substrate were modeled using a surface-to-surface contact formulation. For the contact pressure-overclosure, hard contact was used to implement zero-penetration of the two materials. For the tangential motion, the coefficient of friction of 0.4 was used [32]. The Taylor–Quinney coefficient or inelastic heat fraction was set to 90% of the plastic work [33,34], and 100% of the friction work was converted into heat. The oxide layers were constrained to their respective surfaces to simulate their presence accurately.

Boundary conditions were applied to reflect the physical constraints of the system. The bottom surface of the substrate was fixed, and symmetric boundary conditions were applied to the side surfaces to represent a complete cylindrical geometry.

During the simulation, the particle was accelerated towards the substrate at a constant velocity to mimic the impact process typical in the cold spray technique. The substrate temperature was maintained at an ambient temperature of 25 °C.

Plastic deformations within the system were modeled using the Johnson–Cook model, which is commonly used to predict material behavior under high strain rates [35]. However, the traditional Johnson–Cook model's accuracy diminishes at extremely high strain rates [36]. To address this, a modified Bilinear Johnson–Cook (BJC) model was used:

$$\sigma = (A + B\varepsilon^{n})\left[1 + C ln(1 + \frac{\dot{\varepsilon}}{\dot{\varepsilon}_0})\right]\left[1 - (\frac{T - T_{transition}}{T_{melt} - T_{transition}})^{m}\right] \quad (1)$$

Table 1
Parameters for Bilinear Johnson–Cook model for Ti-based powders [37,38].

J-C Parameter	CP-Ti	Ti–6Al–4V
A [MPa]	390	862
B [MPa]	481.61	331
n	0.319	0.34
C_1	0.0194	0.012
C_2	0.041	0.029
m	0.655	0.8
$T_m[K]$	1933	1974
$\dot{\epsilon}_0$	1	1

$$C = \begin{cases} C_1 & \dot{\varepsilon}_p < \dot{\varepsilon}_c \\ C_2 & \dot{\varepsilon}_p \geq \dot{\varepsilon}_c \end{cases} \quad (2)$$

The BJC model uses two sets of constants for different strain rate regimes, enhancing accuracy at high strain rates.

To implement the BJC model, a subroutine code was developed and integrated into ABAQUS, allowing the simulation of the bi-linear stress–strain behavior of the Ti-based powders during the cold spray process.

The bi-linear Johnson–Cook parameters for CP-Ti and Ti–6Al–4V powders, used in the simulations, were obtained from previous studies and are provided in Table 1 [37,38]. These parameters are crucial for accurately representing the material response and capturing the plastic deformation behavior during impact and bonding.

Brittle cracking criteria, based on Hillerborg et al. [39], were used to model damage in the titanium oxide layers. This approach identifies and removes failed meshes within the oxide layers, representing sections that have cracked or failed due to particle impact.

Oxide behavior was modeled using the Rankine criteria [40], which detects cracks based on tension softening and stiffening, representing Mode I fracture behavior. Crack propagation was assessed using fracture energies for Modes I and II, with key parameters derived from molecular dynamics simulations.

A mesh sensitivity analysis was conducted to ensure the reliability and accuracy of the simulations. This analysis determined that a mesh size of $\frac{1}{50}d_p$ (where d_p is the particle diameter) provided acceptable accuracy with minimal differences in maximum equivalent plastic strain compared to finer mesh sizes.

Adaptive meshing was used to optimize deformation and heat generation modeling near the impact area. The substrate was divided into smaller partitions and meshed according to distance from the top surface, facilitating faster convergence during simulations.

Two sets of finite element simulations were performed: the first explored the effects of topical nano oxide films on crater diameter for both Ti–6Al–4V and CP-Ti powders, while the second investigated the effects of powder impact, particle radius, velocity, and oxide thickness. Analyzing the resulting crater diameters provided insights into these parameters' influence on the cold spray process for Ti-based powders.

A summary of the parameters used in the finite element simulations is provided in Table 2, offering a comprehensive overview of the simulation setup and conditions. The table references experimental works that informed the selected ranges for cold spraying titanium powder.

Damage models were incorporated to capture material behavior during deformation and failure. For Ti–6Al–4V, a Johnson–Cook damage model was employed, which is effective for high strain rate conditions [44]:

$$\bar{\varepsilon}_f^{pl} = \left[d_1 + d_2 exp(d_3 \frac{p}{q})\right]\left[1 + d_4 ln(\frac{\dot{\bar{\varepsilon}}^{pl}}{\dot{\varepsilon}_0})\right]\left(1 + d_5 \frac{T - T_{transition}}{T_{melt} - T_{transition}}\right) \quad (3)$$

Parameters d_1 to d_5 are experimentally measured constants reported by Kay [44], with values of −0.09, 0.27, 0.48, 0.014, and 3.87, respectively.

Table 2
Parameters that are changed to study their effect on the cold spray process.

Parameter [Units]	Range
Impact Velocity, V (m/s) [41]	600, 700, 800, 900[a], 1000, 1100, 1200, 1300
Oxide Thickness, t (nm) [42,43]	1, 2, 3.8[a], 5, 7
Diameter of particle, D (μm)	10, 20, 30[a], 40, 50, 60

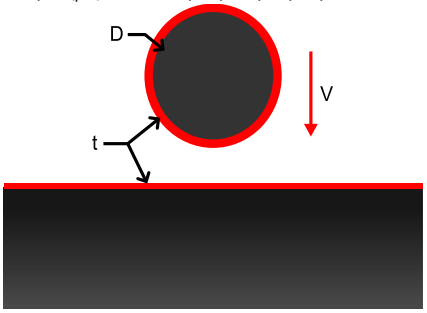

[a] The base numbers used for parameter studies.

For CP-Ti, a ductile damage model was used [45], which predicts crack nucleation and growth based on stress triaxiality and strain rate. The damage criterion is given by:

$$\omega_D = \int \frac{d\bar{\varepsilon}^{pl}}{\bar{\varepsilon}^{pl}_D(\eta, \dot{\bar{\varepsilon}}^{pl})} \tag{4}$$

This model effectively captures the behavior of materials with ductile deformation and failure. Detailed parameters for the CP-Ti ductile damage model can be found in the referenced study.

Incorporating these damage models into the simulations allows an accurate representation of Ti–6Al–4V and CP-Ti responses to deformation and failure under cold spray conditions, providing valuable insights into material behavior during the process.

3. Results

3.1. Oxide characterization and mechanical properties

Using an annealing–quenching method in molecular dynamics, an amorphous structure for titanium oxide was obtained. Fig. 2 illustrates the mean square displacement of the titanium atoms during the annealing step. For the first 1.5 nanoseconds of the simulation, the atoms exhibited a diffusion constant of 4×10^{-9} m^2/s. Despite fluctuations in the diffusion rate, the average rate remained constant during this period. After 1.5 nanoseconds, the diffusion rate dropped to near zero, indicating that the atomic positions stabilized with minor fluctuations.

Following the annealing step, quenching and equilibration were performed. The final structure obtained was used to analyze the partial pair functions for Ti–Ti, Ti–O, and O–O. Fig. 3 displays these pair functions. The peak positions correspond to the nearest neighbor distances. In the Ti–Ti partial pair function, a slight peak is observed before the main peak, indicative of edge-sharing titanium pairs, while the second peak represents corner-sharing pairs. Comparisons across repeated models reveal that the ratio of corner-sharing pairs consistently exceeds that of edge-sharing pairs [46]. However, due to the amorphous nature of the structure, these peaks are less defined compared to those in crystalline titanium oxide (e.g., rutile). In contrast, the O–O pair function lacks distinct edge/corner-sharing features, further confirming the amorphous structure. The nearest neighbor distances in the O–O, Ti–O, and Ti–Ti pairs are 1.92 Å, 2.56 Å, and 3.58 Å, respectively. The higher density of oxygen atoms results in closer packing among oxygen atoms and between oxygen and titanium atoms, whereas the titanium atoms are more shielded by oxygen, leading to a greater distance between titanium atoms.

The average coordination number of titanium atoms was determined from the Ti–O partial pair function by integrating the area under the first peak. This yielded a coordination number of 4.37, consistent with measurements by Petkov et al. [47] for amorphous titanium oxide.

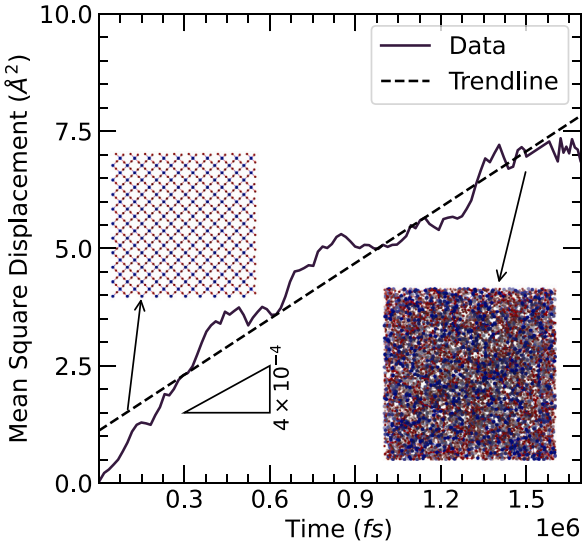

Fig. 2. Mean square displacement plot of Titanium atoms in the titanium oxide structure with respect to time. The trendline shows the diffusion rate of Ti atoms during this simulation.

Angular distribution analysis was performed to assess the average atomic positioning. The major peaks in the Ti–O–Ti angular distribution closely resemble those of crystalline oxides, as noted by Rino et al. [48]. However, the peaks are smaller and more blunt due to the amorphous nature. Fig. 4 shows double peaks in the O–Ti–O, Ti–O–Ti, and Ti–Ti–O angle distributions, reflecting edge-sharing and corner-sharing pairs. The first peak corresponds to edge-sharing pairs, while the subsequent peak represents corner-sharing pairs. Unlike in crystalline systems, these peaks are more dispersed and less pronounced.

It should be noted that although the annealing–quenching method is a rapid approach to obtaining the amorphous structure, it tends to produce an excess of octahedral structures. This is because many interatomic potentials, including the SMTB-Q used here, are optimized for crystalline phases like rutile and anatase, leading to some errors in the results.

Subsequently, a tensile test was conducted on the amorphous structure. The stress–strain curve from this simulation is shown in Fig. 5. The test was performed at two strain rates. Rida et al. [31] indicated that Young's modulus is strain rate-independent below 5×10^5 s^{-1}, while strain rates above this threshold affect Young's modulus. The results demonstrated no significant difference in Young's modulus at strain rates of 10^4 s^{-1} and 10^5 s^{-1}. However, the yield stress increased by approximately 30% at the higher strain rate. Young's modulus for both rates was 42.4 GPa, with ultimate stresses of 1.65 GPa at 10^4 s^{-1} and 2.13 GPa at 10^5 s^{-1}. For finite element analysis, the lower strain rate values were used due to their greater reliability and closer alignment with experimental conditions.

3.2. Influence of topical oxide layers on cold spray process

Previous studies on the impact of titanium particles on titanium substrates have largely overlooked the presence and influence of topical oxide layers [49,50], with few investigations into their effects on other materials [22,51]. Despite their nano-scale thickness, these oxide layers possess significant strength and energy absorption capabilities. As a result, some of the oxide layers may remain intact upon impact. Additionally, small amounts of oxide between the particle and substrate can act as weak links within the system, as the intermolecular interactions between the oxide layer and titanium are weaker than those between

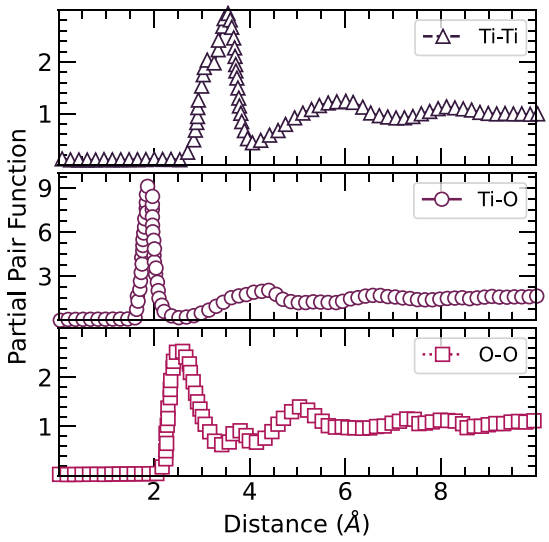

Fig. 3. Partial pair correlation functions for amorphous titanium oxide model obtained from molecular dynamics.

titanium atoms, making fracture initiation more likely at these weak points [52].

Understanding the relationship between impact velocity and particle–substrate interaction is crucial for optimizing the cold spray process and achieving the desired coating properties. Fig. 6 demonstrates how impact velocity affects particle shape, bonding mechanisms, and efficiency. Results show that within the velocity range of 600 to 1200 m/s, the interface between the substrate and particle expands as impact velocity increases, leading to a larger contact area. However, at the highest velocities of 1000 and 1200 m/s, no significant increase in impact area is observed.

Figs. 7a and c illustrate the effect of topical nanosized oxide layers on the splat crater diameter. The presence of a stiff and strong oxide layer limits the compression of the particle compared to particles without TiO_2, resulting in a smaller splat crater diameter when an oxide layer is present. Figs. 7b and d further demonstrate that a portion of the oxide layer remains intact post-impact and is not completely removed by impact or subsequent jetting forces, as similarly observed by Rahmati et al. [22] and Navabi et al. [51]. This indicates that small oxide layers are likely to remain at the interfaces between cold-sprayed powders (CP-Ti or Ti–6Al–4V) and their substrates.

The presence of oxide layers also affects impact-induced temperatures. With an oxide layer present on the particle and substrate surfaces, temperatures do not exceed 990 K for CP-Ti and 1045 K for Ti–6Al–4V, as shown in Fig. 8. These temperatures are significantly lower than those observed without an oxide layer (1183 K for CP-Ti and 1342 K for Ti–6Al–4V). The lower temperatures are attributed to the absorption of kinetic energy by the oxide layer, which is mostly expelled from the interface, resulting in reduced energy absorption by the substrate. The temperature evolution in both titanium grades is similar, though the maximum temperature in CP-Ti is lower due to its higher ductility.

The crater ratio, representing the ratio of the crater diameter to the particle diameter, normalizes the crater size relative to the particle size. For Ti–6Al–4V powders, the crater ratio is 0.78 without an oxide layer and 0.55 with an oxide layer. For CP-Ti powders, the corresponding values are 0.83 without an oxide layer and 0.75 with an oxide layer. This demonstrates the significant energy absorption of the oxide layer and its importance in optimizing cold-spray parameters.

Fig. 9a to 9c show how different parameters affect the crater ratio in the cold spray of CP-Ti or Ti–6Al–4V powders. The presence of a trapped oxide layer, as depicted in Fig. 7, is also noted. The crater ratio increases with impact velocity due to higher particle kinetic energy, leading to greater fracture stress in the oxide layer and a reduced radius of undamaged oxide as impact velocity increases.

Conversely, higher oxide thicknesses result in a lower crater ratio due to the increased energy required to break a thicker oxide layer. The radius of the residual oxide decreases with increased oxide thickness. Finally, the crater ratio slightly decreases with increasing particle diameter, but the ratio of the radius of the residual oxide to the particle diameter remains relatively constant. This is explained by the larger area undergoing pure compression in larger particles, which does not fail during impact.

In summary, Fig. 9 indicates that particle diameter has a modest impact on the final residual oxide, whereas the impact velocity and exposure time of the oxide to ambient air significantly influence the residual oxide in the coated layer.

4. Discussions

The finite element simulations have revealed the substantial impact of nanoscale oxide layers on cold spray impacts (Fig. 7). These oxide layers are crucial for energy absorption before oxide fracture and splat deformation, thereby mitigating impact forces and reducing deformation severity on the substrate. However, the presence of these oxide layers can weaken the adhesion properties between the deposited particles and the substrate, potentially affecting the overall strength and integrity of the cold-sprayed coating.

Stress concentrations around the deposited particles can lead to crack initiation and growth, contributing to potential fatigue failure. These stress concentrations arise from material heterogeneity between the oxide layer and the substrate, geometric irregularities, and interfacial defects, which negatively impact the long-term performance and durability of cold-sprayed coatings.

The interplay between topical oxide layers, adhesion properties, and stress concentrations during cold spray impacts is crucial for optimizing the process and designing coatings with enhanced adhesion and mechanical properties. Different parameters significantly affect crater ratios and unbroken oxide radii (Fig. 9). CP-Ti shows higher crater ratios and lower unbroken oxide radii compared to Ti–6Al–4V, indicating better bonding characteristics for CP-Ti during the cold spray process.

As impact velocity increases, crater ratios tend to increase, while residual oxide radii decrease. This promotes increased bonding due to the compression of the trapped oxide layer and expansion of the bonding area. However, very high velocities can lead to erosion, necessitating a balance to optimize bonding while minimizing material loss.

It is important to recognize the limitations of this disjointed approach at molecular and continuum scales. One significant limitation is the exclusion of grain structure effect and recrystallization [24,53,54]. The grain boundaries in the particles play a crucial role in absorbing impact energy and thus, influence the splat morphology and bonding. Additionally, the current model lacks an accurate representation of yielding and strain-hardening behavior in the substrate. Although the bi-linear Johnson–Cook model is calibrated against experimental data to approximate the material's response, the absence of grain boundaries and grain structures leads to a divergence between the simulation results and the experimental observations. Addressing this discrepancy will require incorporating more advanced modeling techniques, such as crystal plasticity or coupled atomistic-to-continuum (ATC) simulations, to better capture the true material behavior during impact.

Topical oxide layers also influence temperature behavior during the cold spray process. Oxide-coated particles exhibit slower heating rates but eventually reach similar asymptotic temperatures as non-oxide-coated particles. The higher asymptotic temperatures observed for Ti–6Al–4V suggest more favorable conditions for diffusion bonding and geometrical interlocking, enhancing bonding strength [55]. Increased oxide thickness requires more elastic bending before interfacial

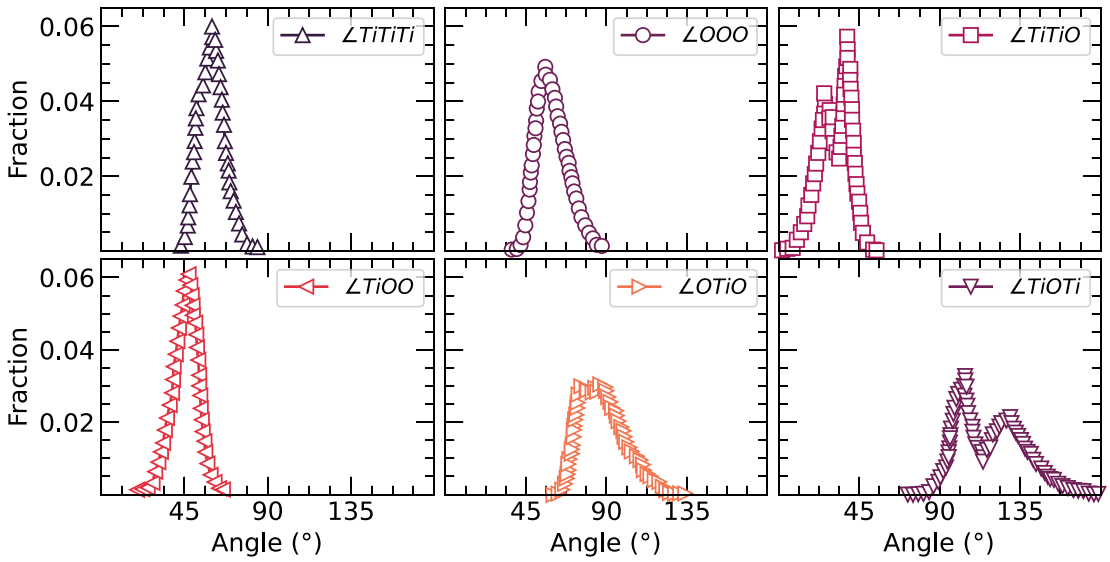

Fig. 4. Normalized density of bond-angle distribution function for possible bonds in the amorphous titanium oxide obtained from molecular dynamics.

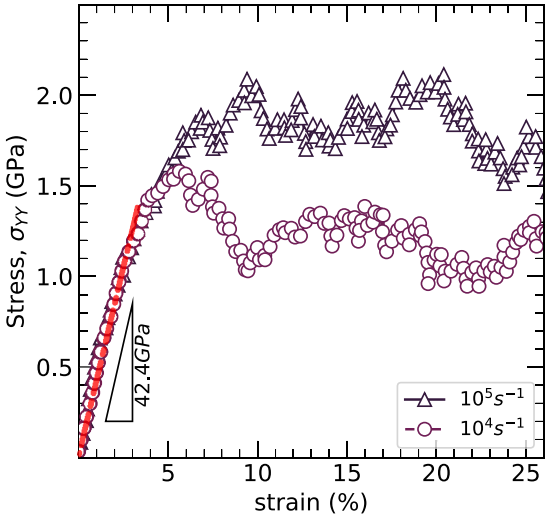

Fig. 5. Normalized density of bond-angle distribution function for possible bonds in the amorphous titanium oxide obtained from molecular dynamics.

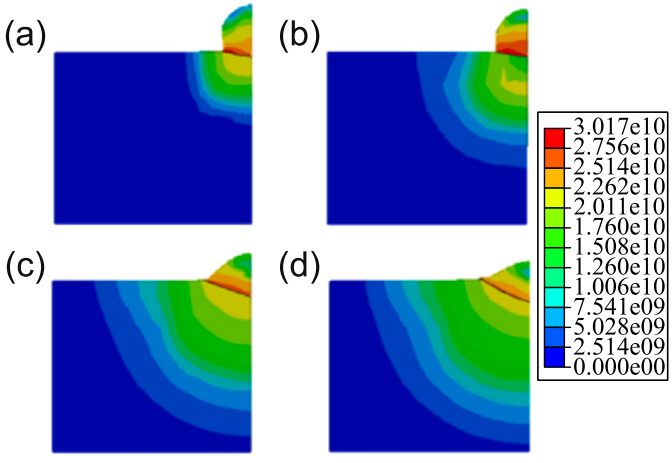

Fig. 6. Particle shape under different impact velocities, (a) 600, (b) 800, (c) 1000, and (d) 1200 m/s.

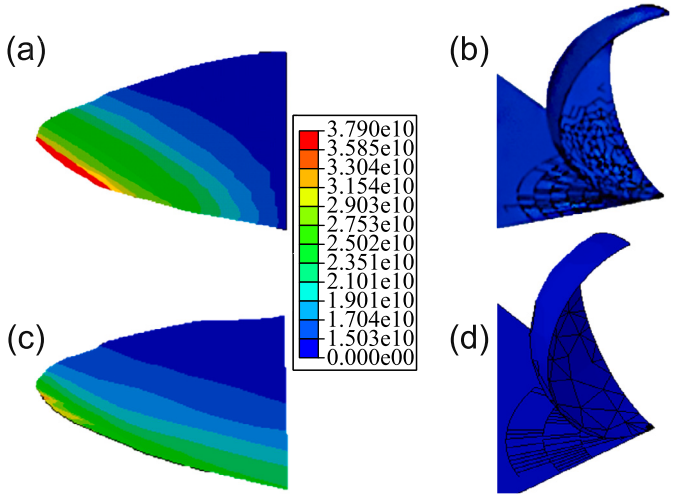

Fig. 7. (a) Stress distribution in the CP-Ti particle at the end of impact, (b) cracks formed in the oxide layer of CP-Ti particle, (c) stress distribution in the Ti–6Al–4V particle at the end of impact, (d) cracks formed in the oxide layer of Ti–6Al–4V particle.

or substrate failure, which reduces the available energy for splat and substrate deformation and decreases crater ratios.

Understanding the slower heat transport through oxide layers compared to crack propagation velocities helps predict and control crack formation, optimizing bonding and adhesion between powders and substrates. The cracking of oxides during cold spray deposition is crucial for bonding and contact between metal particles and the substrate, with metal-on-metal contact occurring in areas where the oxide layer cracks, allowing bonding through diffusion, adhesion, and mechanical interlocking.

However, the brittle nature of oxide layers presents challenges for bonding, as their high strength and low thermal conductivity restrict energy transfer and inhibit strong bond formation. Residual oxide portions between metal particles and the substrate can weaken interfacial strength and limit metal-to-metal contact. The specific characteristics of different Ti alloys and contact parameters influence the behavior of oxide films in Ti alloys, affecting bonding outcomes and the overall performance of sprayed coatings.

To summarize, Fig. 10 presents a schematic of the cold spray process of a single particle impacting the substrate. Unlike the finite element

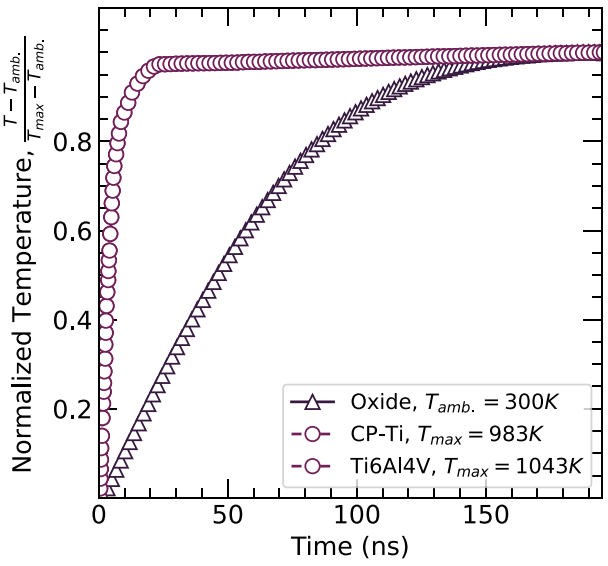

Fig. 8. Temperature evolution in the oxide layer and substrate vs time in CP-Ti and Ti–6Al–4V.

simulations in this work, particles in practice exhibit roughness and sphericity, resulting in further fracture of the oxide layer. Thus, the residual oxide values reported here represent upper estimates. Despite this, controlling particle diameter and optimizing crater ratios enhance contact and bonding between powder particles and substrates in cold spray deposition processes, improving deposition efficiency and coating quality [56]. The presence of nanoscale oxide films profoundly impacts deformation mechanisms and cracking phenomena during cold spray, which is essential for achieving desired coating properties and ensuring the integrity and reliability of the coatings.

5. Conclusion

In summary, this study investigates the effects of topical nanoscale Ti oxides on the cold spray mechanisms of CP-Ti and Ti–6Al–4V powders on substrates with the same material. The key conclusions of the research are as follows:

1. The oxide layers on the surface of the examined powders had an amorphous structure which has lower mechanical properties compared to crystalline TiO_2.
2. CP-Ti, being weaker and more deformable than Ti–6Al–4V, shows larger contact areas, enhancing the bonding in CP-Ti powders during cold spraying compared to Ti–6Al–4V.
3. Deposition efficiency improves as impact velocities increase from 600 to 800 m/s. However, at higher velocities (1000–1200 m/s), there is no significant change in deposition efficiency and contact areas at the substrate-particle interface.
4. Topical nanoscale oxides increase the required critical impact velocities for effectively bonding Ti and Ti–6Al–4V powders to same-material substrates.
5. Residual oxide portions between metal particles and the substrate weaken interfacial strength and limit metal-to-metal contact.
6. Cold spraying of Ti-based powders on same-material substrates involves splat deformation and topical oxide deformation and cracking, resulting in localized heating and temperatures exceeding the recrystallization temperatures of the Ti-based alloys. This allows for diffusion bonding and the formation of deformed surfaces that can conform through geometrical interlocking.

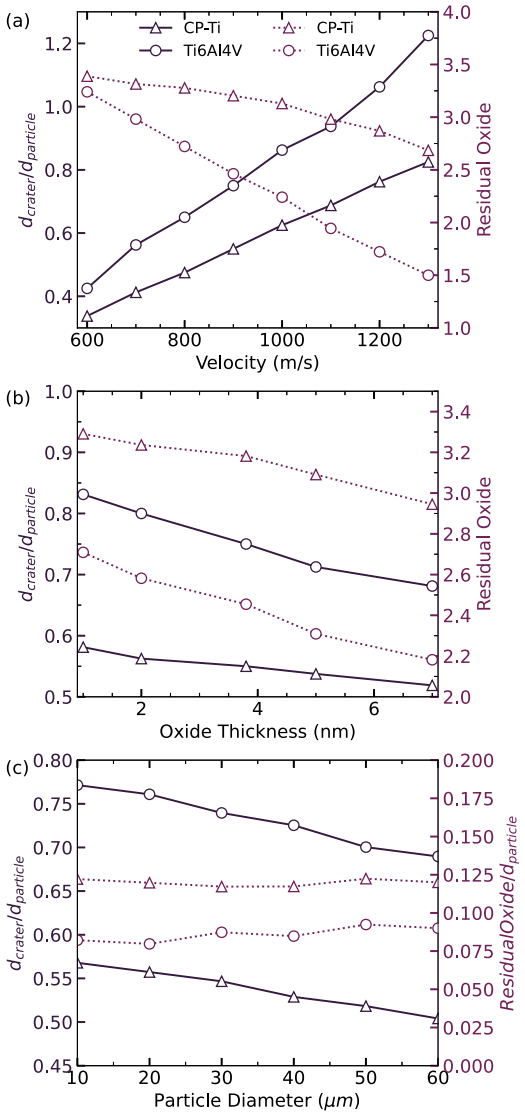

Fig. 9. Results of finite element modeling under different conditions, effect of (a) velocity, (b) oxide thickness, and (c) particle diameter on the crater ratio and radius of the residual oxide.

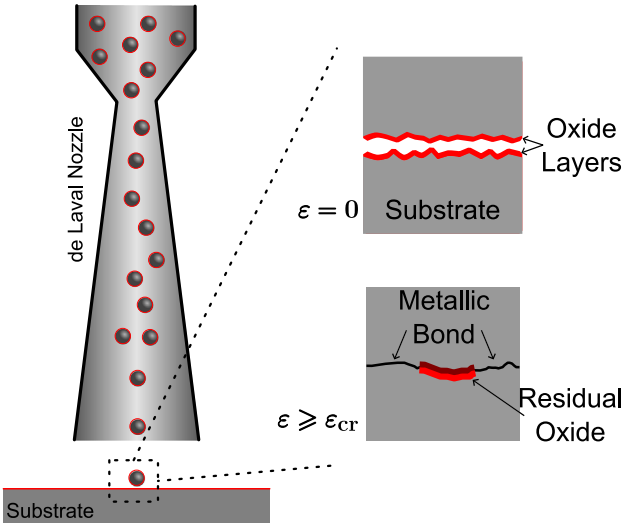

Fig. 10. Schematic of the cold spray process with the surface oxide.

CRediT authorship contribution statement

Mobin Vandadi: Writing – original draft, Visualization, Software, Methodology, Investigation, Data curation. **Trevor Bond:** Methodology, Data curation. **Tabiri K. Asumadu:** Writing – review & editing. **Desmond Klenam:** Supervision. **Nima Rahbar:** Writing – review & editing, Supervision, Project administration, Funding acquisition, Conceptualization. **Winston Soboyejo:** Writing – review & editing, Supervision, Project administration, Conceptualization.

Declaration of competing interest

The authors declare that they have no known competing financial interests or personal relationships that could have appeared to influence the work reported in this paper.

Acknowledgments

We acknowledge the support from the DEVCOM Army Research Laboratory Grant No. W911NF22-2-0040. The authors acknowledge support from Dr. Kevin Doherty, Program Manager, for his enormous encouragement and advice. The Harvard Center for Nanoscale Systems is also acknowledged for experimental work on the focus ion beam and TEM data.

Data availability

Data will be made available on request.

References

[1] M. Vandadi, D. Klenam, N. Rahbar, W. Soboyejo, Advances in the structural integrity of cold sprayed alloys - a critical review of process models and mechanical properties, in: Reference Module in Materials Science and Materials Engineering, 2022.
[2] M. Leshetla, et al., Corrosion resistance of iron-containing experimental titanium alloys exposed to simulated body fluids, Mater. Corros. 73 (8) (2022) 1298–1307.
[3] J. Donachie, Titanium: A Technical Guide. Metals Park, ASM International, 1988.
[4] O.E. Pohler, Unalloyed titanium for implants in bone surgery, Injury 31 (2000) D7–D13.
[5] M. Niinomi, Mechanical properties of biomedical titanium alloys, Mater. Sci. Eng. A 243 (1–2) (1998) 231–236.
[6] R.R. Boyer, An overview on the use of titanium in the aerospace industry, Mater. Sci. Eng. A 213 (1–2) (1996) 103–114.
[7] C. Leyens, M. Peters, Titanium and Titanium Alloys: Fundamentals and Applications, John Wiley & Sons, 2003.
[8] I. Weiss, S. Semiatin, Thermomechanical processing of beta titanium alloys—an overview, Mater. Sci. Eng. A 243 (1–2) (1998) 46–65.
[9] V. Krishnan, K.J. Kumar, Mechanical properties and surface characteristics of three archwire alloys, Angle Orthod. 74 (6) (2004) 825–831.
[10] E. Mohseni, et al., Ti/TiN/HA coating on Ti–6Al–4V for biomedical applications, Ceram. Int. 41 (10) (2015) 14447–14457.
[11] F. Froes, B. Dutta, The Additive Manufacturing (AM) of Titanium Alloys, vol. 1019, Trans Tech Publ, 2014.
[12] A.P. Alkhimov, A.N. Papyrin, V.F. Kosarev, N.I. Nesterovich, M.M. Shushpanov, Gas-dynamic spraying method for applying a coating, 1994, Google Patents, US Patent 5, 302, 414.
[13] A. Tokarev, Structure of aluminum powder coatings prepared by cold gasdynamic spraying, Metal Sci. Heat Treat. 38 (3) (1996) 136–139.
[14] D. Klenam, et al., Cold spray coatings of complex concentrated alloys: Critical assessment of milestones, challenges, and opportunities, Coatings 13 (3) (2023) 538.
[15] P. Cavaliere, A. Silvello, Crack repair in aerospace aluminum alloy panels by cold spray, J. Therm. Spray Technol. 26 (2017) 661–670.
[16] D. Guo, et al., Cold spray: Over 30 years of development toward a hot future, J. Therm. Spray Technol. 31 (4) (2022) 866–907.
[17] R.F. Vaz, A. Garfias, V. Albaladejo, J. Sanchez, I.G. Cano, A review of advances in cold spray additive manufacturing, Coatings 13 (2) (2023) 267.
[18] A. Kumar, D.K. Goyal, R. Kant, H. Singh, Enhancing corrosion performance of cold-sprayed Titanium/Baghdadite (Ti/BAG) Bio-composite coatings via laser treatment, Coatings 12 (7) (2022) 1010.
[19] V. Champagne, D. Helfritch, Critical assessment 11: structural repairs by cold spray, Mater. Sci. Technol. 31 (6) (2015) 627–634.
[20] H. Assadi, F. Gärtner, T. Stoltenhoff, H. Kreye, Bonding mechanism in cold gas spraying, Acta Mater. 51 (15) (2003) 4379–4394.
[21] A. Hemeda, et al., Particle-based simulation of cold spray: Influence of oxide layer on impact process, Addit. Manuf. 37 (2021) 101517.
[22] S. Rahmati, R.G. Veiga, A. Zuniga, B. Jodoin, A numerical approach to study the oxide layer effect on adhesion in cold spray, J. Therm. Spray Technol. 30 (7) (2021) 1777–1791.
[23] R. McCune, A. Papyrin, J. Hall, I. Riggs, P. Zajchowski, et al., An Exploration of the Cold Gas-Dynamic Spray Method for Several Materials Systems, Techreport, ASM International, Materials Park, OH (United States), 1995.
[24] S.H. Zahiri, D. Fraser, M. Jahedi, Recrystallization of cold spray-fabricated CP titanium structures, J. Therm. Spray Technol. 18 (1) (2009) 16–22.
[25] M. Mindel, S. Pollack, The room temperature oxidation of titanium thin films, Acta Metall. 17 (12) (1969) 1441–1448.
[26] E. Gemelli, N. Camargo, Oxidation kinetics of commercially pure titanium, Matéria (Rio de Janeiro) 12 (2007) 525–531.
[27] H. Zhang, B. Chen, J.F. Banfield, G.A. Waychunas, Atomic structure of nanometer-sized amorphous TiO 2, Phys. Rev. B 78 (21) (2008) 214106.
[28] A.P. Thompson, et al., LAMMPS-a flexible simulation tool for particle-based materials modeling at the atomic, meso, and continuum scales, Comput. Phys. Comm. 271 (2022) 108171.
[29] E. Maras, N. Salles, R. Tétot, T. Ala-Nissila, H. Jónsson, Improved tight-binding charge transfer model and calculations of energetics of a step on the rutile TiO2 (110) surface, J. Phys. Chem. C 119 (19) (2015) 10391–10399.
[30] A.K. Rappe, W.A. Goddard III, Charge equilibration for molecular dynamics simulations, J. Phys. Chem. 95 (8) (1991) 3358–3363.
[31] A. Rida, M. Micoulaut, E. Rouhaud, A. Makke, Understanding the strain rate sensitivity of nanocrystalline copper using molecular dynamics simulations, Comput. Mater. Sci. 172 (2020) 109294.
[32] L. Meier, N. Schaal, K. Wegener, In-process measurement of the coefficient of friction on titanium, Procedia CIRP 58 (2017) 163–168.
[33] G.I. Taylor, H. Quinney, The latent energy remaining in a metal after cold working, Proc. Royal Soc. Lond. Ser. A Contain. Pap. Math. Phys. Character 143 (849) (1934) 307–326.
[34] A. Stroh, A theoretical calculation of the stored energy in a work-hardened material, Proc. R. Soc. A 218 (1134) (1953) 391–400.
[35] A.A. Dehkharghani, Tuning Johnson–Cook Material Model Parameters for Impact of High Velocity, Micron Scale Aluminum Particles, Northeastern University, 2016.
[36] X. Wang, et al., Dynamic behavior and a modified Johnson–Cook constitutive model of Inconel 718 at high strain rate and elevated temperature, Mater. Sci. Eng. A 580 (2013) 385–390.
[37] D.R. Lesuer, G. Kay, M. LeBlanc, Modeling Large-Strain, High-Rate Deformation in Metals, Techreport, Lawrence Livermore National Lab.(LLNL), Livermore, CA (United States), 2001.
[38] X. Wang, M. Hassani, Ultra-high strain rate constitutive modeling of pure titanium using particle impact test, J. Appl. Mech. 87 (9) (2020).
[39] A. Hillerborg, M. Modéer, P.-E. Petersson, Analysis of crack formation and crack growth in concrete by means of fracture mechanics and finite elements, Cem. Concr. Res. 6 (6) (1976) 773–781.
[40] W.J.M. Rankine, II. On the stability of loose earth, Philos. Trans. R. Soc. Lond. (147) (1857) 9–27.
[41] T. Schmidt, F. Gärtner, H. Assadi, H. Kreye, Development of a generalized parameter window for cold spray deposition, Acta Mater. 54 (3) (2006) 729–742.
[42] R. Shvab, E. Hryha, L. Nyborg, Surface chemistry of the titanium powder studied by XPS using internal standard reference, Powder Metall. 60 (1) (2017) 42–48.
[43] E. Hryha, R. Shvab, M. Bram, M. Bitzer, L. Nyborg, Surface chemical state of ti powders and its alloys: Effect of storage conditions and alloy composition, Appl. Surf. Sci. 388 (2016) 294–303.
[44] K. Gregory, Failure Modeling of Titanium 6Al-4V and Aluminum 2024-T3 with the Johnson–Cook Material Model, vol. 9, US William J. Hughes Technical Center, Washington, 2003.
[45] J. Zhai, et al., Modeling the ductile damage process in commercially pure titanium, Int. J. Solids Struct. 91 (2016) 26–45.
[46] B. Prasai, B. Cai, M.K. Underwood, J.P. Lewis, D. Drabold, Properties of amorphous and crystalline titanium dioxide from first principles, J. Mater. Sci. 47 (21) (2012) 7515–7521.
[47] V. Petkov, G. Holzhüter, U. Tröge, T. Gerber, B. Himmel, Atomic-scale structure of amorphous TiO2 by electron, X-ray diffraction and reverse Monte Carlo simulations, J. Non-Cryst. Solids 231 (1–2) (1998) 17–30.
[48] J.-P. Rino, N. Studart, Structural correlations in titanium dioxide, Phys. Rev. B 59 (10) (1999) 6643.
[49] F. Rubino, A. Astarita, P. Carlone, Thermo-mechanical finite element modeling of the laser treatment of titanium cold-sprayed coatings, Coatings 8 (6) (2018) 219.
[50] T.D. Phan, S.H. Masood, M.Z. Jahedi, S.H. Zahiri, Residual stresses in cold spray process using finite element analysis, in: Materials Science Forum, Vol. 654, Trans Tech Publ, 2010, pp. 1642–1645.
[51] A. Navabi, et al., Deformation and cracking phenomena in cold sprayed 6061 Al alloy powders with nanoscale aluminum oxide films, Mater. Sci. Eng. A 841 (2022) 143036.

[52] J. Ramier, et al., Cohesion and adhesion of nanoporous TiO2 coatings on titanium wires for photovoltaic applications, Thin Solid Films 516 (8) (2008) 1913–1919.
[53] P. Vo, et al., Cold-spray processing of titanium and titanium alloys, in: Titanium Powder Metallurgy, Elsevier, 2015, pp. 405–423.
[54] Z. Li, et al., Microstructure evolution and mechanical behavior of cold-sprayed, bulk nanostructured titanium, Metall. Mater. Trans. A 45 (2014) 5017–5028.
[55] O. Ivasishin, P. Markovsky, Y.V. Matviychuk, S. Semiatin, Precipitation and recrystallization behavior of beta titanium alloys during continuous heat treatment, Metall. Mater. Trans. A 34 (1) (2003) 147–158.
[56] K. Binder, J. Gottschalk, M. Kollenda, F. Gärtner, T. Klassen, Influence of impact angle and gas temperature on mechanical properties of titanium cold spray deposits, J. Therm. Spray Technol. 20 (1) (2011) 234–242.